Local Analysis of Flooding in Jianghua County, Yongzhou City Based on Remote Sensing Data

Zhijun Hua

Reading Academy, Nanjing University of Information Science & Technology, Nanjing, Jiangsu Province, 210000, China

202283700009@nuist.edu.cn

Abstract. Floods are one of the common natural disasters. Due to the accumulation and growth of water levels caused by natural and artificial factors, floods often cause damage to farmland and construction land and casualties. Currently, remote sensing is developing rapidly and has strong advantages in dynamic monitoring of flood disasters. This article selects the microwave data of Sentinel-1 SAR, combined with the land cover type and population data of ESA and JRC, to conduct change detection and disaster analysis and assessment of the flood that occurred in Qingtang Zhuang Nationality Town, Jianghua County, Yongzhou City, Hunan Province, China in June 2022. This study detected the range of obvious flood changes in the study area by analyzing different image data, and provided an initial assessment of the potential impact of floods on land types and population. Research results show that floods in Qingtang Zhuang Nationality Town mainly occurred in cultivated land and a small part of forestland areas in the central area, and affected a small proportion of people. The research results provide certain references for regional flood detection and disaster analysis. Further research can combine more data, such as terrain slope, to conduct a more detailed visualization of the affected features.

Keywords: Flood, remote sensing, change detection, disaster analysis.

1. Introduction

Flooding is when a water body rises above its regular level, often threatening the safety of areas along rivers, lake shores and near the sea, and even causing inundation disasters. Flooding is due to excessive natural precipitation or insufficient drainage, causing property damage, casualties, building collapse and other phenomena. The danger of flooding to human society and production should not be ignored. Floods not only inundate low-lying areas but also damage crops, drown livestock, destroy houses, and affect commercial activities, schools, monuments and relics, water and electricity supplies, and the spread of diseases. China has a vast territory with diverse natural geographic conditions. The uneven distribution of precipitation in time and space has led to frequent droughts and floods. According to statistics, between 1991 and 2017, more than 150 billion of direct economic losses in China came from floods yearly [1]. Therefore, effective prevention and control measures are needed to reduce their impacts.

Flood disasters are characterised by a high degree of suddenness and hazardousness. The large inundated area caused by the outbreak of floods is dynamically changing, so real-time dynamic monitoring of the affected area is particularly important in disaster relief. Satellite remote sensing technology, which has the characteristics of strong timeliness and wide coverage, has been widely used in assessing floods. Remote sensing can quickly monitor the flooded area and invert a variety of physical elements, providing certain support and reference for the rapid response to floods and disaster assessment [2, 3]. In recent years, with the multispectral, hyperspectral, infrared, synthetic aperture radar (SAR), night-light, and other remote sensing technology for earth observation continues to progress, remote sensing imaging means tend to be more diverse, which also improves the accuracy of the detection of natural disasters such as floods. However, there are some differences in image resolution, field of view, and the nature of the target for the same feature in a given scene with multi-source remote sensing images. There is redundancy and complementarity in the data provided by multiple sources [4]. This requires ion of data from different sources to achieve more accurate and comprehensive monitoring and analyses for the subject of the study.

This paper aims to detect changes and assess the hazard in the local flooded area in Yongzhou City, Hunan Province, China, from 20 to 22 June 2022 based on multi-source remote sensing data. This study focuses on the dynamic monitoring of flooding with the help of Google Earth Engine (GEE) using multiple remote sensing data from Sentinel-1 SAR, the European Space Agency (ESA), and Joint Research Centre (JRC).

2. Data and Methods

2.1. Overview of the study area

This article uses Jianghua County, Yongzhou City, Hunan Province, China as the study area. Fig. 1 shows the geographical location of Yongzhou City in China. Yongzhou City is located in the southwestern part of Hunan Province. It is dominated by hills and mountains, with 14.29 per cent plains and 17.81 per cent granite, 4.51 per cent hills and 49.45 per cent mountains. The Xiangjiang River flows through the north of Yongzhou, and the Xiaoshui River joins the Xiangjiang River from south to north. The city has a total area of 22,259 square kilometres and a total resident population of about 5.15 million [5].

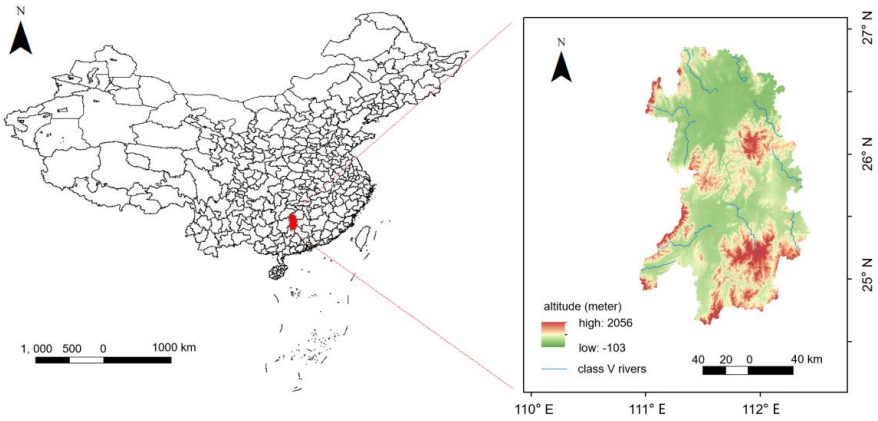

Figure 1. Location of Yongzhou City in China

Jianghua Yao Autonomous County is located south of Yongzhou City (Fig. 2). The county has a total area of 3,248 square kilometres, with a total population of 537,800, of which 340,000 are Yao nationality, and a forest coverage rate of 78.78 per cent, with a standing wood volume of more than 16 million cubic metres, and more than 500,000 acres of primary and primary secondary forests.

Figure 2. Study area in Jianghua County - Qingtang Zhuang Nationality Town

In this study, Qingtang Zhuang Nationality Town of Jianghua County (111°71" E - 111°76′ E, 24°94′ N - 24°99′ N), located in the central part of Jianghua Yao Autonomous County, Yongzhou City, Hunan Province, with a total area of 32 km2, was selected for the study of flood change. At the end of 2011, the total population of this area was 7,275 people.

From 20 June 2022 to 22 June 2022, Jianghua County, Yongzhou City, Hunan Province, sustained heavy to very heavy rainfall, locally very heavy rainfall. Four towns in Jianghua County, namely, Weizhukou Township, Daxi Township, Yashi Township and Daxu Township, were the main areas affected by the flood. The flash floods caused 72 houses to collapse, 246 houses to collapse, 122 houses to collapse, 341 houses to collapse, 350 houses to collapse, 965 houses to collapse, and 8,090 hectares of crops to collapse. Trasportation, communication, and electricity were all interrupted in the most seriously affected townships, Yashichi, Weizhukou, and Daxi, and the direct economic loss reached 1.723 billion yuan [6].

2.2. Data Source

GEE is a cloud-based computing platform for processing satellite imagery and other Earth observation data. The platform provides global-scale data access and processing capabilities, including online visualisation, computation and analytical processing of satellite images and Earth observation data. Microwave remote sensing data, land cover type data and global population distribution data were selected for this study.

The microwave image data are based on Sentinel-1 SAR GRD data from the database integrated in GEE.Sentinel-1 is a radar satellite of the ESA, funded by the European Union and operated by the space mission in the Copernicus programme. Sentinel-1 collects C-band SAR images in a variety of polarisations and resolutions images. SAR, through its altimeter, can provide water level measurements of almost all inland rivers and lakes around the clock, providing flood level data for flood-affected areas [7]. The selection of such microwave images allows for more efficient identification and display of water bodies and is less susceptible to cloud interference.

The land cover type data is ESA WorldCover 10 m 2020 in the GEE database. This data provides a global land cover map for 2021 at a resolution of 10 m based on Sentinel-1 and Sentinel-2 data. The WorldCover product contains 11 land cover classes and was generated within the framework of the ESA WorldCover project, which is a part of the ESA's 5th Earth Observation Envelope Programme (EOEP-5) [8].

The global population data is derived from the GHSL: Global population surfaces 1975-2030 (P2023A) data from the JRC data integration of the GEE platform data. This raster dataset describes the spatial distribution of the residential population, expressed as the absolute number of inhabitants in a cell. Residential population estimates for the period 1975 to 2020 were obtained at 5-year intervals, and projections for 2025 and 2030 were obtained based on CIESIN GPWv4.11. These population estimates were disaggregated from census or administrative units to grid cells, which were delineated with reference to the distribution, volume and classification of built-up areas for each epoch in the GHSL Global Built-up Area Surface Layer [9].

2.3. Research Methods

The change detection method plays a vital role in flood mapping, which uses remotely sensed data to identify and map flooded areas. This method can efficiently and accurately assess the extent of a flood event and provide some support for disaster response and management efforts [10]. In this paper, the difference method is used for flood change detection. Due to the short transit time of the flood, the images of the flood need to be time-sensitive, which requires a high temporal resolution of the selected data, and high resolution images are at the same time susceptible to the interference of clouds and fog. Therefore, the choice of microwave imagery is more appropriate for flood recognition. This is because microwave images can identify and display water bodies more efficiently and are less susceptible to cloud interference. This paper selects two polarisation modes, VV and VH, from the Sentinel-1 SAR at 5.405 GHz (C band) with a resolution of 10 m for the analysis. The wavelength of the C band is about 5 cm, which is an excellent choice to consider both the feature information and the penetration capability [11]. Its applications are mainly precipitation, cloud and soot penetration, soil moderation monitoring and flood mapping [12]. VV and VH are two common polarisations in SAR images. The sensors of remote sensing satellites transmit vertically polarised waves and receive

either vertically polarised (VV) or horizontally polarised (VH) waves. These two polarisations have different characteristics in different applications. VV polarized SAR images have better penetration capabilities in areas with higher surface roughness (such as vegetation), so they are more common when observing areas such as forests and grasslands. VH-polarised SAR images have better reflection in areas with lower surface roughness (e.g., bodies of water, buildings), and are therefore more common when observing areas such as bodies of water and cities.

Firstly, the research chooses the microwave remote sensing images from 1 May to 1 June 2022 and 10 June to 25 June 2022, with the polarisation of "VV" and the mode of "IW". Due to the noise interference, edge denoising of the image data is required. At the same time, the "VH" band, which is the most effective in identifying water bodies, is selected to acquire flood images of the study area. The "VH" value of the flooded area is lower than that of the area before flooding, so the difference between the "VH" values before and after flooding can be used to reflect the flooding changes. Considering that there are negative values in the VH values, it is necessary to normalise the obtained VH difference to obtain an image that reflects the severity of the flood.

For the acquisition of land cover types in the study area, the ESA WorldCover 10 m 2020 data was selected [8]. This ESA product provides global land cover maps for 2020 at a resolution of 10 m, based on the Sentinel-1 and Sentinel-2 data. The WorldCover product consists of 11 land cover categories. The dataset includes 11 categories with values ranging from 10 to 100, including trees, shrubs, grassland, cropland, buildings, and other land cover types. This dataset was imported into GEE to crop the land use categories for the study area and to calculate the area values for each land use category in the study area at a resolution of 10 metres.

In addition, the JRC global population dataset of GHSL: Global population surfaces 1975-2030 (P2023A) was used in this study to obtain the population size and distribution of the study area by cropping the images and calculating the total population in the area with the help of the sum of the pixels in the cropped image [9]. Fig. 3 shows the flow chart of the research methods used in this paper:

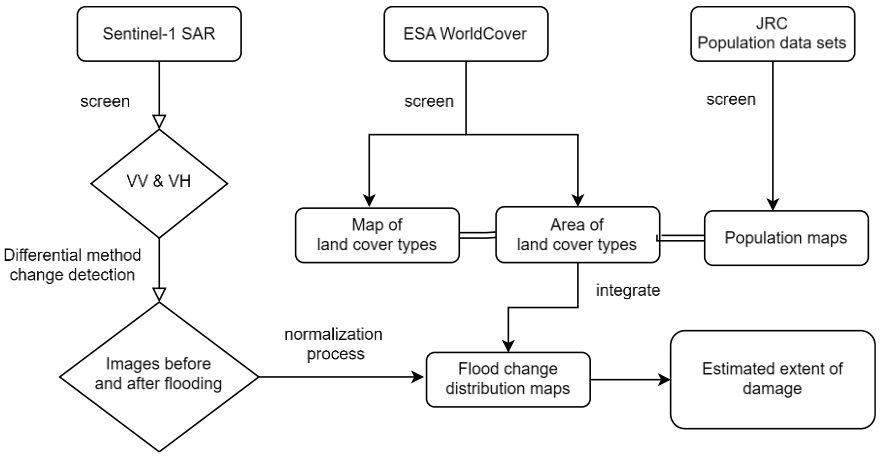

Figure 3. Flowchart of the research methods

3. Results

3.1. Visualization of land cover types

The results of the land use classification in the study area are shown in Fig. 4. Six bands with values of 10, 30, 40, 50, 60 and 80 were included in the study area, while the rest of the bands were not counted because they did not exist or were too small in size. This means that the main types of land in the area are trees, grassland, arable land, buildings, bare land and permanent water bodies. The following graphs (Fig. 4 and Table 1) show that the study area is mountainous and hilly, with a high degree of terrain undulations, vegetation cover, and a low level of development. The tree type occupies the largest area of land at 69.33 per cent. This is followed by arable land and grassland with less built-up area, while a small portion of water bodies are present

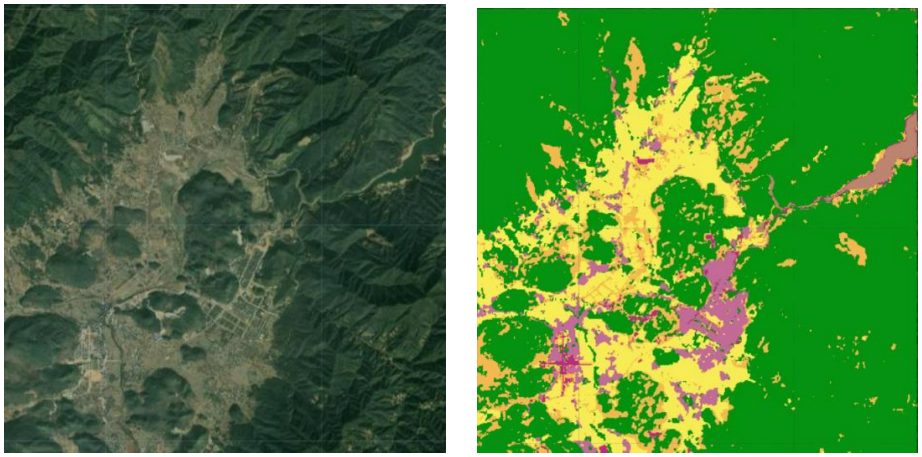

(a) (b)

Figure 4. Land cover types in Qingtang Zhuang Nationality Town: (a) true-colour image; (b) land classification

Table 1. Land cover types in Qingtang Zhuang Nationality Town

Value	Color	Land cover type	Area (m2)	Proportion
10		Tree	57540327	69.33%
30		Grass	8214485	9.89%
40		Cropland	11947953	14.40%
50		Construction	3781249	4.56%
60		Bare	702945	0.85%
80		Permanent water bodies	803045	0.97%

3.2. Visualization of population size and distribution

The study of population size and distribution was carried out with the help of JRC global population dataset. The study resulted in an image of population distribution in the study area as shown in Fig.5. Lighter colours indicate higher population density. It can be seen that the population is mainly distributed in the central as well as south-western parts of the study area. The location of the higher population density in this image corresponds well with the location of the distribution of grass, shrubs and buildings in the image of the land distribution types in the area. The region is in a mountainous area with significant drop-offs and a low population distribution, which was calculated to be approximately 19,520 people in this range. However, the accuracy of the obtained population images is still not high enough, which is related to the fact that the range of the selected population dataset is too large.

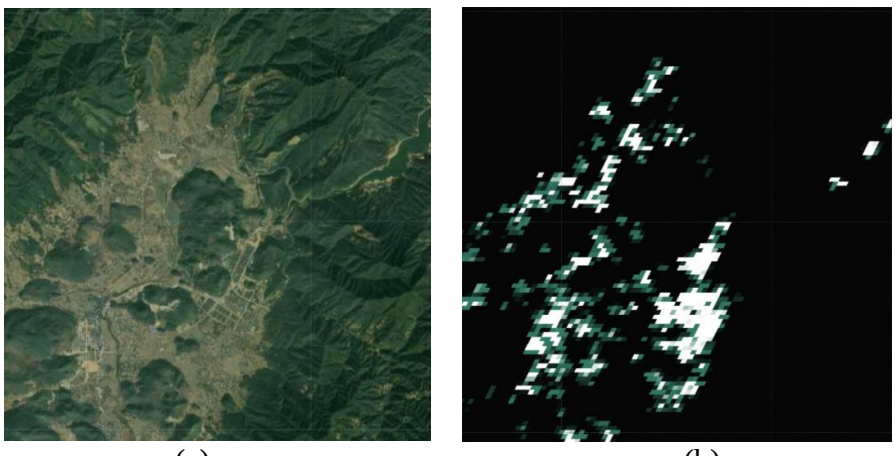

(a) (b)

Figure 5. Population distribution map of Qingtang Zhuang Nationality Town: (a) true-colour image; (b) population distribution

3.3. Visualisation of flood change detection

The microwave remote sensing images obtained by Sentinel-1 SAR were analysed, and the two images on the left (Fig. 6) showed that the dark-coloured part of the water body had been expanded to a certain extent after the flood. Through the normalised difference method of change detection, it can be found that the part with more extensive changes is the original part of the water body. By combining the land cover types and population distribution in the area shown above (Fig. 4 and 5), it can be concluded that the floods mainly affected some of the cultivated and forested land in the central part of the study area, and only a very small portion of the building land was disturbed by the floods. In addition, the region's population is concentrated in the west and south, so only a small number of residents live in the more severely flooded areas, and the number of people affected is small.

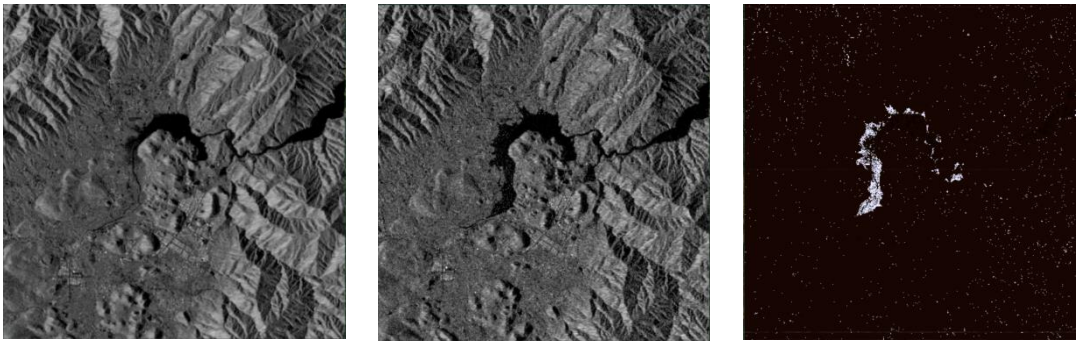

(a) (b) (c)

Figure 6. Flood change detection: (a) Pre-flood microwave image; (b) Post-flood microwave image; (c) Flood change distribution

Based on the analysis of all the images presented above, some suggestions can be made for the prevention of future floods. First, the floods are more likely to affect some of the cultivated and forested land located in the lower part of the terrain. In the future development plan of the area, it is possible to increase the planting of trees on the slopes, set up flood dams, build terraces, and change the distribution of the original land cover types to reduce the impact of flooding on the land used for cultivation and residential use. In addition, according to the scope of the flood and population distribution, the government can make full use of the existing roads or new roads to provide emergency evacuation routes and resettlement places for the residents in the area to achieve the minimisation of casualties in floods and the rapid and orderly evacuation of emergencies.

4. Conclusion

This article uses Sentinel-1 SAR, ESA land classification, and JRC global population data to reflect the changes of flooding in Qingtang Zhuang Nationality Town, Jianghua County, Yongzhou City, Hunan Province in June 2022, and to analyse and assess the risk of flooding in relation to the distribution of land cover types and population in the area. The Sentinel-1 SAR microwave remote sensing data with "VV" and "VH" cross-polarisation were used to pre-process the images before and after the flooding in the study area, such as denoising, and then using the difference method and normalisation for flood detection to highlight the severely flooded areas. Flooding affects mainly part of the arable land and the built-up area, but only a small part of the study area. The population within this area is primarily located in the arable and built-up areas. The flood-prone areas did not occur in the more densely populated areas, and the number of people affected by the floods was small. Such population distribution is more conducive to post-flood rescue and reconstruction. Among the three types of remote sensing image acquisition, the image quality of Sentinel-1 for flood change detection and ESA for a land cover type is higher, and they fit well with each other and with satellite remote sensing images. Although the accuracy of the population data from JRC is low, it can match well with the original remote sensing images, and a preliminary analysis and assessment can be made. In subsequent studies, the acquired images can be used to visualise the area, number of people affected

and the distribution of land types affected by floods. In addition, in the detection of flood changes, we can consider combining the JDR permanent water body and DEM data for more objective and scientific analyses, as well as combining the factors of terrain slope for more accurate detection to provide better support and suggestions for flood disaster relief and flood damage analysis.

References

[1] Yang, K. Progress, Challenge and Prospect for Remote Sensing Monitoring of Flood and Drought Disasters in China. IEEE INTERNATIONAL GEOSCIENCE AND REMOTE SENSING SYMPOSIUM, 2019, 4280-4283.

[2] Li, S. S., Li, J. C., Zhang, X. D., Zhou, T., Zhong, W. and Li, X. Application of Beijing series high-resolution satellites in flood analysis of the Yongding River Basin. China Water, 2024, 69-72.

[3] Liu, X. Y., Cui, Y. P., Shi, Z. F., Fu, Y. M., Run, Y. D., Li, M. D., Li, N. and Liu, S. J. Monitoring of floods using multisource remote sensing images on the GEE platform. National Remote Sensing Bulletin, 2023, 27 (9): 2179-2190.

[4] Li, S. T., Li, C. Y. and Kang. X. D.. Development status and future prospects of multi-source remote sensing image fusion. National Remote Sensing Bulletin, 2021, 25 (1): 148-166.

[5] Yongzhou National Economic and Social Development Statistics Bulletin (n.d.). Government Data. [online] Available at: http://www.yzcity.gov.cn/cnyz/shuj/zfsj.shtml [Accessed 16 Feb. 2024].

[6] The Paper. Five Typical cases, Flash Flood Disaster Prevention Capabilities Have Been Further Improved, 2023 [online] Available at: https://www.thepaper.cn/gov_112134 [Accessed 26 Feb. 2024].

[7] CU Xiaoye, LI Xiaotao, SU Qiaomei, MA Jianwei, SONG Wenlong, XU Jiaxin. Progress of synthetic aperture radar altimeter application. Water Resources and Hydropower Technology, 2023.

[8] Zanaga, D., Van De Kerchove, R., Daems, D., De Keersmaecker, W., Brockmann, C., Kirches, G., Wevers, J., Cartus, O., Santoro, M., Fritz, S., Lesiv, M., Herold, M., Tsendbazar, N.E., Xu, P., Ramoino, F. and Arino, O. ESA WorldCover 10 m 2021 v200, 2022.

[9] Schiavina, M., Freire, S., Alessandra, C., MacManus, K. GHS-POP R2023A - GHS population grid multitemporal (1975-2030). European Commission, Joint Research Centre (JRC), 2023.

[10] Ahmed, Y.G., Ateeq ur, R., Fahad, R., Muhammad, M. and Ghani, R. Flood Mapping Using the Sentinel-1 SAR Dataset and Application of the Change Detection Approach Technique (CDAT) to the Google Earth Engine in Sindh Province, Pakistan. Ecological Questions, 2024, 35 (2).

[11] SPACE WILL. Selection of SAR Images in Different Application Scenarios, 2023, [online] Available at: https://www.spacewillinfo.com/news/xingyexinwen/2023/0421/589.html [Accessed 3 Mar. 2024].

[12] ESRI. (n.d.). Introduction to Synthetic Aperture Radar. [online] Available at: https://pro.arcgis.com/zh-cn/pro-app/3.0/help/analysis/image-analyst/introduction-to-synthetic-aperture-radar.htm [Accessed 3 Mar. 2024].